Korean J. Chem. Eng., 35(2), 421-427 (2018)
DOI: 10.1007/s11814-017-0267-y

pISSN: 0256-1115
eISSN: 1975-7220

Reduction of CO_2 to CO via reverse water-gas shift reaction over CeO_2 catalyst

Bican Dai*, Shiquan Cao*, Hongmei Xie*, Guilin Zhou*,,†, and Shengming Chen***

*Chongqing Key Laboratory of Catalysis & Environmental New Materials, Department of Materials Science and Engineering, College of Environment and Resources, Chongqing Technology and Business University, Chongqing 400067, China
**Engineering Research Center for Waste Oil Recovery Technology and Equipment, Ministry of Education, Chongqing 400067, China
(*Received 19 June 2017 • accepted 25 September 2017*)

Abstract−CeO_2 catalysts with different structure were prepared by hard-template (Ce-HT), complex (Ce-CA), and precipitation methods (Ce-PC), and their performance in CO_2 reverse water gas shift (RWGS) reaction was investigated. The catalysts were characterized using XRD, TEM, BET, H_2-TPR, and *in-situ* XPS. The results indicated that the structure of CeO_2 catalysts was significantly affected by the preparation method. The porous structure and large specific surface area enhanced the catalytic activity of the studied CeO_2 catalysts. Oxygen vacancies as active sites were formed in the CeO_2 catalysts by H_2 reduction at 400 °C. The Ce-HT, Ce-CA, and Ce-PC catalysts have a 100% CO selectivity and CO_2 conversion at 580 °C was 15.9%, 9.3%, and 12.7%, respectively. The highest CO_2 RWGS reaction catalytic activity for the Ce-HT catalyst was related to the porous structure, large specific surface area (144.9 $m^2 \cdot g^{-1}$) and formed abundant oxygen vacancies.

Keywords: Cerium Oxide Catalyst, Carbon Dioxide, Carbon Monoxide, Reverse Water-gas Shift (RWGS) Reaction, Oxygen Vacancy

INTRODUCTION

The concentration of the major greenhouse gas, CO_2, is significantly increasing in the atmosphere because of combustion emissions of fossil fuels. This increase results in global warming, melting glaciers, and drowning coastal cities. However, CO_2 is also an affordable, nontoxic, and abundant C1 (i.e., carbon element or a molecule containing a carbon atom) raw material. CO_2 reduction is accepted as one of the most effective ways for CO_2 utilization to reduce CO_2 concentration in the atmosphere. However, the CO_2 molecule is linear with a double bond between carbon and oxygen atoms (O=C=O), which results in high thermodynamic and chemical stability [1,2]. Moreover, CO_2 reduction requires high-energy electron donors. H_2 is also accepted as a high-energy electron donor. Abundant H_2 can be produced by water electrolysis and photo-assisted decomposition of water [3]. Therefore, creating a new energy source or C1 raw material by CO_2 catalytic hydrogenation is the most attractive and challenging way to synthesize chemicals. Reverse water-gas shift (RWGS), methanation, and MeOH synthesis are classified as hydrogenation. RWGS is the most attractive method and offers the most promising hydrogenation reaction. CO_2 can be converted into a more active CO by RWGS reaction, which can be used to synthesize alkanes, olefin, alcohols, aldehyde, and acid by the Fischer-Tropsch reaction [1].

RWGS, which is the reverse reaction of water-gas shift, is less investigated because of less actual demand. The investigation of RWGS reaction progressed in the 1990s when the international community began to focus on energy efficiency and a wide range of environmental issues. Yoshihara et al. [4] investigated RWGS kinetics over Cu(110) model catalysts and found that RWGS was strongly structure sensitive. Moreover, MoS_2 and WS_2 have better CO selectivity than Fe, Co, and Ni supported on Al_2O_3 in RWGS reaction [5]. Some papers have also reported that RWGS plays a vital role in many chemical processes, such as carbon neutral cycle [6-8]. Thus, enhancing the efficiency of RWGS is essential.

CeO_2 is a typical rare earth metal oxide that has a face-centered cubic fluorite structure. CeO_2 species can be reduced to form a series of uncertain $CeO_{2-\delta}$ species with an oxygen defect structure in reduction atmosphere. Moreover, CeO_2 can maintain a fluorite crystal structure even if it is converted into $CeO_{2-\delta}$ with oxygen vacancy [9,10]. However, $CeO_{2-\delta}$ species can be oxidized by oxidizing substances to form CeO_2. Furthermore, CeO_2 can be reduced by H_2 to form Ce_2O_3 and generate abundant oxygen vacancies [11]. The formed oxygen vacancies can be oxidized by CO_2 to release CO [12,13]. Therefore, CeO_2 as support to catalytic RWGS reaction has recently been investigated. NiO/CeO_2 catalyst has been investigated in RWGS reaction by CeO_2 redox properties [14]. The Pt/CeO_2 catalyst has been investigated because the support CeO_2 can generate a strong interaction with Pt to promote its catalytic performance for the RWGS reaction [15,16]. However, studies about the CO_2 RWGS reaction over CeO_2 catalysts are still seldom reported so far.

Usually, the structure of the solid catalyst is directly affected by the preparation methods, and the catalytic performances can also be affected by the structure. The hard-template method can play a good role in creating pores to improve the porosity and surface area of the corresponding catalyst. The result was confirmed in our previous work [17,18]. The advantage of the typical complex method and the precipitation method is that the preparation of catalyst is

†To whom correspondence should be addressed.
E-mail: dicpglzhou@ctbu.edu.cn, upcglzhou@sohu.com

convenient. And, the composition of catalyst is easy to control using the typical complex method [18]. At present, studies about RWGS reaction over CeO_2 catalysts with the different structure are clearly unknown. We synthesized CeO_2 catalysts with different structural properties using the different preparation methods. The synthesized CeO_2 catalysts were used to catalyze the RWGS reaction. The physical and chemical properties of the prepared CeO_2 catalysts were investigated using X-ray diffraction (XRD), transmission electron microscopy (TEM), Brunauer-Emmett-Teller (BET), H_2-temperature programmed reduction (H_2-TPR) analyses, and in-situ X-ray photoelectron spectroscopy (XPS).

EXPERIMENTAL

1. Catalyst Preparation

The CeO_2 catalysts were prepared by the hard-template method, the typical complex method, and the typical precipitation method, respectively. The experimental details have been described in our previous reports [17,18]. Here, these methods are briefly described. In the typical the hard-template method, $Ce(NO_3)_3{\cdot}6H_2O$ was dissolved in ethanol, and then KIT-6 mesoporous silica was added. The KIT-6 mesoporous silica hard template was prepared according to the procedure described by our previous report [2]. The mixture was stirred until a dry power was obtained. The power was dried, followed by calcination. The impregnation procedure was repeated once, followed by calcination. The obtained samples were treated with NaOH to remove template. The obtained product was designated as Ce-HT.

In the typical complex method synthesis process, $Ce(NO_3)_3{\cdot}6H_2O$ and citric acid were dissolved in a certain amount of deionized water. The mixture was then stirred until the deionized water completely evaporated. Afterwards, the sample was dried, followed by calcination. The obtained product was designated as Ce-CA.

In the typical precipitation method synthesis process, $Ce(NO_3)_3{\cdot}6H_2O$ was dissolved in a certain amount of deionized water. Subsequently, dilute ammonia was added until the pH of the solution reached to 9. The precipitate then was aged, centrifuged, and washed until the pH value was less than 7.5. Finally, the sample was dried, followed by calcination. The obtained product was designated as Ce-PC.

2. Catalyst Characterization

2-1. XRD Characterization

X-ray diffraction (XRD) patterns were obtained on a Rigaku D/Max-2500/PC diffractometer with a rotating anode using Ni filtered Cu-Ka as radiation source (λ=0.15418 nm) at 40 kV of a tube voltage and 200 mA of a tube current. The diffraction patterns were collected from 20° to 80° at the rate of 5° min^{-1}.

2-2. TEM Analysis

Transmission electron microscopy (TEM) was performed using a Tecnai G^2 Spirit microscope operating with an acceleration voltage of 120 kV. For the TEM observation, the samples were first dispersed in ethanol under ultrasonication, followed by evaporation on to a carbon-coated copper grid.

2-3. BET Characterization

The adsorption-desorption isotherms of the samples were collected on a Micromeritics ASAP 2020 automatic analyzer at −196 °C. The samples were degassed under vacuum at 200 °C for 3.0 h prior to the measurement. Based on adsorption data, the Brunauer-Emmett-Teller (BET) method was used to calculate the specific surface area.

2-4. H_2-TPR Studies

Hydrogen temperature programmed reduction (H_2-TPR) was carried out using a conventional apparatus equipped with a TCD detector. In a typical process, 30 mg of the sample was placed in a U-type quartz tube (4.0 mm i.d.). Subsequently, TPR was performed by heating the samples from room temperature to 650 °C at the heating rate of 10 °C/min, in the presence of 5% H_2/Ar mixture flowing at the rate of 25 ml/min.

2-5. *In-situ* XPS Characterization

The chemical states of the Ce-HTH (Ce-HTH: Ce-HT catalyst were reduced *in-situ* in an high-purity H_2 in at 400 °C) and Ce-HTO (Ce-HTO: Ce-HTH was oxidized *in-situ* in CO_2 for 30 min at 320 °C) were determined using *in-situ* X-ray photoelectron spectroscopy (*in-situ* XPS). The XPS signals were collected using an ESCALAB 250Xi analyzer. Ce 3d and O 1s binding energies (BEs) were recorded using Al $K\alpha$ ($h\nu$=1,486.6 eV) as the excitation source, and a passing energy of 20 eV. The C 1s signal at 284.6 eV was taken as a reference for BE calibration.

3. Catalytic Activity Tests

The CO_2 RWGS reaction was used to investigate catalytic performance of the preparation Ce-HT, Ce-CA, and Ce-PC catalysts. Before the RWGS reaction, the CeO_2 catalysts were reduced *in-situ* in an high-purity H_2 stream at 400 °C for 2.0 h and at a heating ramp rate of 10 °C/min, followed by cooling under a H_2 flow to the given temperature. The RWGS catalytic tests of all catalysts were performed at atmospheric pressure in a continuous flow fixed-bed quartz tubular reactor (6 mm i.d.). The quartz tube reactor containing 50 mg catalyst was then placed inside the tubular furnace. The actual reduction and reaction temperatures were measured using a thermocouple directly inserted into the catalyst bed and monitored by a temperature programmable controller (ÜGU, model 708P, China). The reaction temperature ranged from 300 °C to 580 °C. The feed gas mixture consisting of CO_2 (10.0 vol%), H_2 (40.0 vol%), and Ar (50.0 vol%) was passed through the catalysts at a flow rate of 50 ml·min^{-1}, which is equivalent to a gas mass space velocity of 60,000 ml·g^{-1}·h^{-1}. The CO_2 conversion and productions selectivity data were obtained and repeated at a given temperature for 120 min. The gas products were analyzed using a packed TDX-01 column with an on-line gas chromatograph (GC 6890II) equipped with a thermal conductivity detector (TCD). The conversions of CO_2 and CO selectivity were calculated according to the following equations:

$$CO_2\ \text{conversion} = \frac{[CO_2]_{inlet} - [CO_2]_{outlet}}{[CO_2]_{inlet}} \times 100\% \quad (1)$$

$$CO\ \text{selectivity} = \frac{[CO]_{outlet}}{[CO]_{outlet} + [CH_4]_{outlet}} \times 100\% \quad (2)$$

RESULTS AND DISCUSSION

1. XRD Characterization

Fig. 1 shows XRD patterns of the Ce-HT, Ce-CA, and Ce-PC

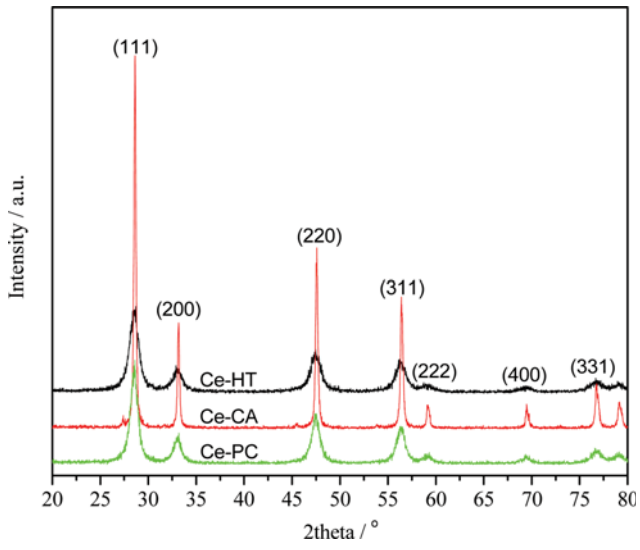

Fig. 1. XRD patterns of the Ce-HT, Ce-CA, and Ce-PC catalysts.

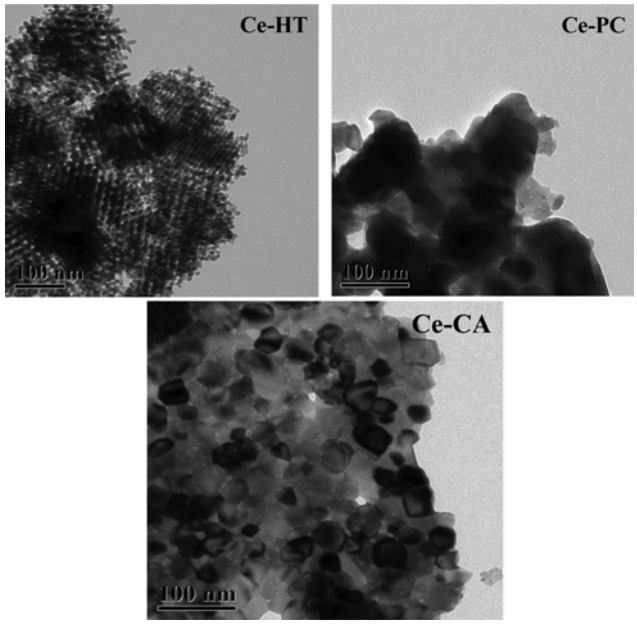

Fig. 2. TEM images of the Ce-HT, Ce-CA, and Ce-PC catalysts.

catalysts prepared by the different preparation methods. The Ce-HT, Ce-CA, and Ce-PC catalysts display eight intense and sharp diffraction peaks. These typical peaks at 2θ=28.56°, 33.11°, 47.59°, 56.41°, 59.18°, 69.52°, 76.69°, and 79.23° are associated with the typical characteristic peaks of CeO_2. On the one hand, eight distinct XRD peaks agree with the {111}, {200}, {220}, {311}, {222}, {400}, {331}, and {420} planes of the face-centered cubic fluorite structure (space group *Fm*-3*m*) of CeO_2; these peaks were indexed using standard data (JCPDS 34-0394) [19]. Moreover, the diffraction peaks of the other cerium compounds were not observed. On the other hand, XRD diffraction peaks of the Ce-CA catalyst are the strongest and narrowest. XRD diffraction peaks of the Ce-PC catalyst are relatively stronger and narrower than those of the Ce-HT catalyst. Therefore, the Ce-CA catalyst has a higher crystallinity than the Ce-PC and Ce-HT catalysts. The crystallinity of the Ce-HT catalyst is the worst. Poor crystallinity results in the Ce-HT catalyst generating more crystal defects. Crystal defects function as reaction activity centers for catalytic and reduction reactions.

2. TEM Analysis

The TEM images of the Ce-HT, Ce-CA and Ce-PC catalysts prepared by different synthetic methods are shown in Fig. 2. The Ce-HT catalyst displays a well-ordered mesoporous structure of the typical KIT-6 with a 3D and symmetrically-ordered mesoporous structure. The result indicates that the Ce-HT catalyst is a perfectly duplicated KIT-6, and the pore structure of Ce-HT is the removal of template skeletal structure. These results, reported by Djinović et al. [20], are consistent with our previous report [18]. Porous structure is conducive to reactant molecule adsorption and activation, which promotes reactant molecules to contact and react with the Ce-HT catalyst. However, the porous structure of the Ce-CA and Ce-PC catalysts is not evident. The Ce-CA catalyst shows a loosely aggregated uniform particle structure with a clear size and shape. The Ce-PC catalyst shows an overlapped and piled-up bulk structure where the particles gather and stick closely to each other, which results in the formation of larger aggregation particles with distinct shapes and sizes. These results can be ascribed to different prepared methods (i.e., citric acid complex and precipitation methods). A large amount of gas can be produced and released in the citric acid complex method. Thus, the obtained catalyst structure is loose and particle size is small. Grain growth is difficult to control, and large-diameter particles are formed using precipitation method. Moreover, the aggregated uniform particle structure of the Ce-CA catalyst and the overlapped and piled-up bulk structure of the Ce-PC catalyst are unfavorable to reactant molecule adsorption and activation unlike the Ce-HT catalyst with a mesoporous structure. Therefore, the Ce-CA and Ce-PC catalysts may have a relatively low catalytic activity during the catalytic reaction.

3. BET Characterization

The nitrogen adsorption-desorption isotherms of the Ce-HT, Ce-CA, and Ce-PC catalysts are shown in Fig. 3. The adsorption-

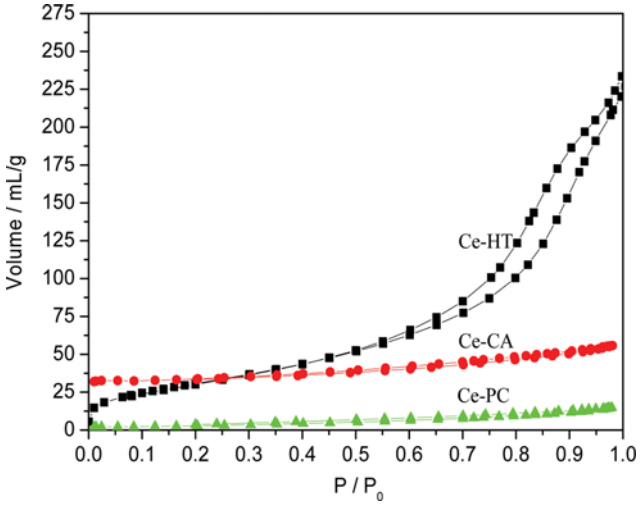

Fig. 3. N_2 adsorption-desorption isotherms of the Ce-HT, Ce-CA, and Ce-PC catalysts.

desorption isotherm of the Ce-HT catalyst is typically Type IV, which is similar to the IUPAC classification with type-H3 hysteresis loop, thereby indicating that the Ce-HT catalyst has a slit-shaped mesoporous structure [21]. The average pore diameter of the Ce-HT catalyst is about 20 nm. The absorbance of the nitrogen molecules when P/P_0 ranges from 0.75 to 0.95 sharply increases because of capillary condensation [22]. These results can be explained by effective replication of KIT-6 structure by the developed porous structure of the Ce-HT catalyst, which was confirmed by the results of TEM. The specific surface area of the Ce-HT catalyst obtained by the BET equation is 144.9 $m^2 \cdot g^{-1}$.

However, the N_2 adsorption-desorption isotherms of the Ce-CA and Ce-PC catalysts are almost straight lines without a hysteresis loop, and the N_2 adsorption capacity is low. The Ce-CA catalyst's adsorption quantity when P/P_0 reaches 1.00 is only about 48.0 ml/g, and Ce-PC catalyst's adsorption quantity is only close to 12.5 ml/g. The values imply that the catalysts have a very weak affinity toward the adsorbed N_2 gas molecules. The specific surface areas of the Ce-CA and Ce-PC catalysts obtained by the BET equation are 32.0 and 11.0 $m^2 \cdot g^{-1}$, respectively. Combined with the TEM results, the Ce-CA catalyst has an agglomerated structure. Moreover, the Ce-PC catalyst has an overlapped bulk structure with low porosity.

The specific surface area of the Ce-HT catalyst is about five times more than that of the Ce-CA catalyst and about 13 times more than that of the Ce-PC catalyst. Therefore, the porous structure and large specific surface area of the Ce-HT catalyst can better enhance the adsorption capacity of reactant molecules and activate the molecules compared with the Ce-CA and Ce-PC catalysts.

4. H_2-TPR Studies

Fig. 4 shows the H_2-TPR profiles of the Ce-HT, Ce-CA, and Ce-PC catalysts. The Ce-HT catalyst shows two reduction peaks at 115 °C to 450 °C and 450 °C to 650 °C, respectively. The Ce-CA catalyst shows two reduction peaks at 120 °C to 300 °C and 300 °C to 600 °C, respectively. Two reduction peaks of the Ce-PC catalyst appear at 150 °C to 300 °C and 300 °C to 600 °C, respectively. The Ce-HT, Ce-CA, and Ce-PC catalysts have significantly different low-temperature reduction peaks. The Ce-HT catalyst shows a wide and intense low-temperature reduction peak at 115 °C to 450 °C. The Ce-CA catalyst shows a very weak peak at 120 °C to 300 °C. The Ce-PC catalyst shows a relative narrow and weak peak at 150 °C to 300 °C.

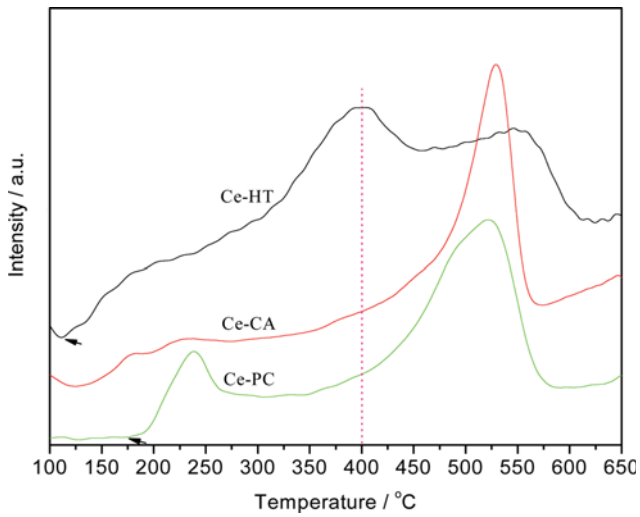

Fig. 4. H_2-TPR profiles of the Ce-HT, Ce-CA, and Ce-PC catalysts.

The low-temperature reduction peak of the CeO_2 samples reduces surface oxygen, and the high-temperature reduction peak reduces lattice oxygen. Therefore, the reduction peaks of the Ce-HT, Ce-CA, and Ce-PC catalysts at 115 °C to 450 °C, 120 °C to 300 °C, and 150 °C to 300 °C, respectively, can be attributed to the reduction of surface oxygen species [23]. The reduction peaks of Ce-HT, Ce-CA, and Ce-PC catalysts at 450 °C to 650 °C, 300 °C to 600 °C, and 300 °C to 600 °C respectively, can be attributed to the reduction of the lattice oxygen of CeO_2 [24]. Furthermore, better reducibility corresponds to lower reduction temperature. The H_2 consumption curves of the Ce-HT, Ce-CA, and Ce-PC catalysts start to deviate from the baseline at about 115, 120, and 150 °C, respectively. The result indicates that the reducibility of the Ce-HT, Ce-CA, and Ce-PC catalysts at low temperature follows the order Ce-HT>Ce-CA>Ce-PC. According to the results of the TEM and BET, the Ce-HT catalyst has a porous structure and a large specific surface area, which is conducive for H_2 molecules to adsorb and react with surface oxygen species on the surface of the CeO_2 catalyst. The Ce-HT catalyst has the worst crystallinity based on the XRD results and is likely to be reduced by H_2 to form oxygen vacancy. Thus, the Ce-HT catalyst has an excellent low-temperature reducibility, which makes it easily reducible by H_2. The area of reduction peak corresponds to the consumed amount of hydrogen. The amount of hydrogen consumption is calculated by the integrated areas of hydrogen consumption peaks and the consumed amount of hydrogen of Ce-HT, Ce-CA, and Ce-PC at low temperature of 100-450 °C is 2.38 mmol/g, 0.45 mmol/g, and 0.68 mmol/g, respectively. The amount of hydrogen consumption corresponds to the content of reducible oxygen species in the CeO_2. The consumed amount of hydrogen of Ce-HT, Ce-CA, and Ce-PC at low temperature follows the order Ce-HT>Ce-PC>Ce-CA. The result indicates that the content of low-temperature reducible oxygen species follows the order Ce-HT>Ce-PC>Ce-CA. The amount of low-temperature H_2 consumption of Ce-HT is the largest among the studied catalysts. Thus, abundant surface oxygen species of the Ce-HT catalyst can be reduced by H_2 reduction at low temperature.

5. *In-situ* XPS Characterization

The *in-situ* XPS spectra of Ce3d for the Ce-HTH and Ce-HTO are shown in Fig. 5(a). The Ce3d XPS peaks at 882.02, 887.79, 897.51, 899.59, 906.78, and 915.82 eV are attributed to Ce^{4+}. The peaks that correspond to Ce^{4+} can be observed in the Ce-HTH and Ce-HTO. The peak intensity and position that correspond to Ce^{4+} do not change in Ce-HTO like those in Ce-HTH. Moreover, no peaks that correspond to Ce^{3+} are observed in Ce-HTH. Therefore, Ce_2O_3 is not formed after CeO_2 is reduced by H_2 at 400 °C [25]. The *in-situ* XPS spectra of O1s for Ce-HTH and Ce-HTO are shown in Fig. 5(b). The peak at 528.49 eV to 530.51 eV is attributed to lattice oxygen (O_{Latt}), and the peak at 531.01 eV to 532.51 eV is attributed to the surface oxygen (O_{Sur}) [26]. The two-type peaks of oxygen are observed in the Ce-HTH and Ce-HTO, and O_{Sur} peaks are observed at 531.75 eV in Fig. 5(b). Moreover, the intensity of the peak that corresponds to O_{Sur} increased in Ce-HTO. The peak

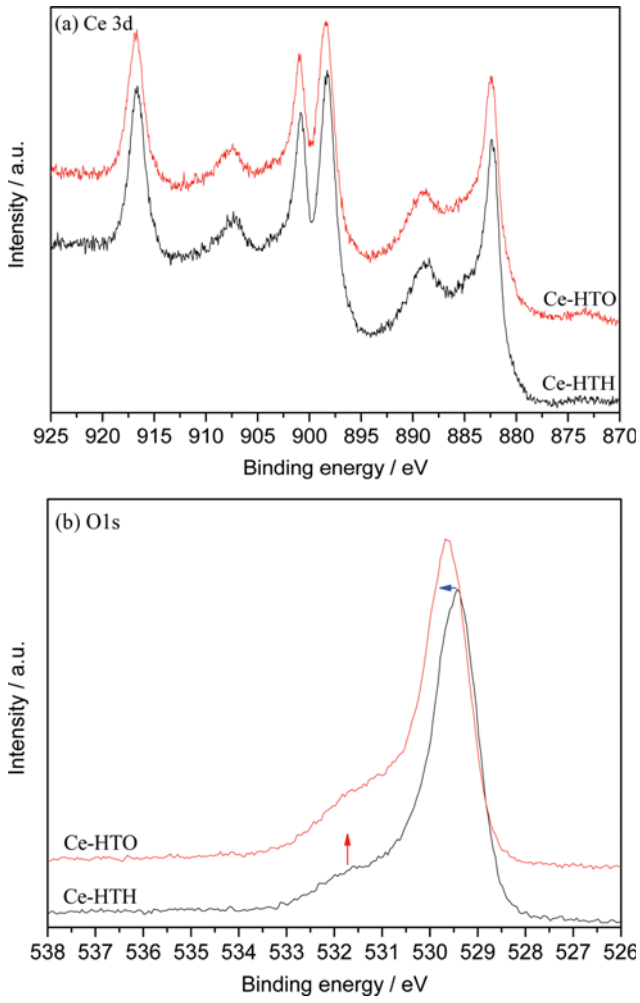

Fig. 5. *In-situ* XPS spectra of (a) Ce3d and (b) O1s for the Ce-HTH and Ce-HTO.

for Ce-HTO at 529.53 eV is attributed to O_{Latt} without intensity increment in Fig. 5(b). The peak for Ce-HTH in Fig. 5(b) shows that the peak of O_{Latt} is observed at 529.30 eV, and the displacement of 0.23 eV occurs in the direction of low binding energy.

The peak intensity and position of O species is consistent with its content and chemical environment. The peak position of O_{Latt} occurring displacement in the Ce-HTH implies that the chemical environment around O_{Latt} changed compared with the Ce-HTO. Oxygen vacancy and/or Ce_2O_3 may be formed when H_2 reduced CeO_2. The formed oxygen vacancy is neutral on the surface of the CeO_2, and two electrons remain the same [27]. If the two electrons transfer to the Ce^{4+} close to the vacancy site, then Ce^{4+} can be reduced to Ce^{3+}. However, Ce_2O_3 is not generated when the Ce-HT catalyst is reduced by H_2 at 400 °C. This finding is based on the *in-situ* XPS spectra of the Ce3d and XRD results under the studied conditions. These results indicate that an oxygen vacancy with two electrons can be formed in the Ce-HTH, which increases the cloud density of the O1s outer electron. According to the atomic electrostatic model, the increase of the O1s outer electron cloud density leads to the shielding effect of the outer electron when the inner electron increases [28]. On the other hand, the electron binding energy of O_{Latt} decreases with the increase of the shielding effect of the outer electron on the O1s inner electron. Therefore, the changed chemical environment around O_{Latt} can be attributed to the form of oxygen vacancies in Ce-HTH. Thus, oxygen vacancies can be formed when Ce-HT is reduced by H_2 at 400 °C. The increment of the peak intensity of O_{Sur} for Ce-HTO indicates that the content of O_{Sur} increases. Therefore, the formed oxygen vacancies in Ce-HTH can be oxidized by CO_2 molecules [11]. Hence, the oxygen vacancies can be recovered, which results in the increment of O_{Sur} content for Ce-HTO. The following hypothesis was obtained: CeO_2 cannot be reduced to form Ce_2O_3 by H_2 at 400 °C, and only the O_{Sur} can be reduced to generate the oxygen vacancy, which can be oxidized by CO_2. The oxygen vacancies that are produced by H_2 reduction can improve the catalytic activity of the CeO_2 catalyst in the catalytic reaction. To further confirm this hypothesis, the H_2-TPR of Ce-HTO was performed and the results are provided in the Supporting Information. From Fig. S1 in the supporting information, two reduction peaks (α and β) are observed at about 400 °C and 550 °C for the studied samples, respectively, which can be assigned to the reduction of surface oxygen species and lattice oxygen. As can be seen in Fig. S1, the α peak area for the Ce-HTH is obviously smaller than that of the Ce-HT, indicating that surface oxygen species were reduced to form the oxygen vacancies by H_2 at 400 °C [11]. And, the α peak area of the Ce-HTO is obviously larger than that of the Ce-HTH, indicating that the oxygen vacancies can be oxidized by CO_2, which well agrees with the *in-situ* XPS results. Based on the TPR results, the Ce-HT catalyst can be more easily reduced by H_2 to form abundant oxygen vacancies at a low temperature, which can be conducive to catalytic reaction.

6. Catalytic Activity Test

Fig. 6 shows the CO_2 conversion on the prepared Ce-HT, Ce-CA, and Ce-PC catalysts. And, the yield of CO_2 to CO for the studied CeO_2 catalysts is also shown in the Fig. 6 illustration. CO_2 conversion increases with the increase of reaction temperature over Ce-HT, Ce-CA, and Ce-PC catalysts. When the reaction temperature increases from 300 °C to 580 °C, the CO_2 conversion on the Ce-HT, Ce-CA, and Ce-PC catalysts increases from 1.2% to 15.9%, 0.4% to 9.3%, and 0.5% to 12.7%, respectively. The thermodynamic equi-

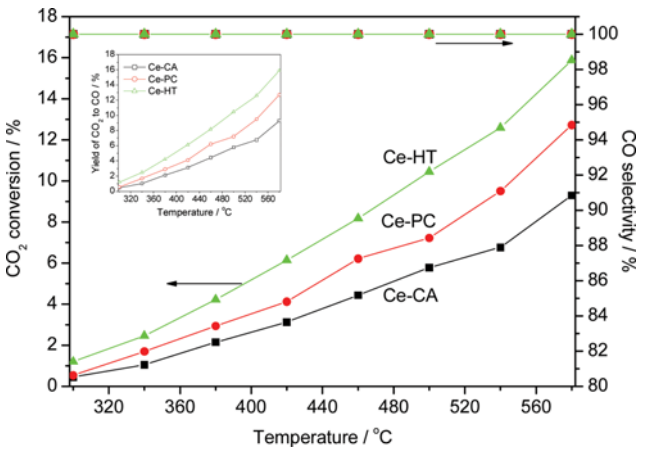

Fig. 6. CO_2 conversion and CO yield on the prepared Ce-HT, Ce-CA, and Ce-PC catalysts.

librium conversion of the RWGS reaction obtained from the literature is 26.4% and 63.3% at 300 °C and 580 °C, respectively [29]. Obviously, the CO_2 conversion on the studied CeO_2 catalysts is far less than the thermodynamic equilibrium conversion at 300 °C and 580 °C. The Ce-CA catalyst shows the lowest CO_2 conversion and is 54% less than the thermodynamic equilibrium conversion at 580 °C. The Ce-HT catalyst exhibits the highest CO_2 RWGS catalytic activity and is the closest to the thermodynamic equilibrium among the studied catalysts in the range of 300 °C to 580 °C. The CO_2 conversion over the Ce-HT catalyst is about 1.7-times higher than that over the Ce-CA catalyst at 580 °C. Moreover, CO selectivity over the studied CeO_2 catalysts is at 100%. As has been reported, the Cu/SiO_2 and Fe/SiO_2 catalysts realized a 100% CO selectivity, but showed a low CO_2 RWGS activity about 8.1% and 2.5% at 600 °C, respectively [30]. The Ni catalysts in CO_2 RWGS showed a higher activity at 500 °C than the CeO_2 catalysts, but only moderate CO selectivity (about 30-50%) [14]. The Ce-HT catalyst showed a high CO_2 conversion and its selectivity to the CO can reach to 100% under a wide temperature range. Therefore, the Ce-HT catalyst is promising for the CO_2 RWGS reaction.

CO_2 can be converted into CO on the appropriate catalyst via RWGS reaction. The conversion is expressed as $CO_2+H_2 \rightarrow CO+H_2O$. The by-product CH_4 may be produced in the process of the CO_2 reduction (i.e., $CO_2+4H_2 \rightarrow CH_4+2H_2O$, $CO+3H_2 \rightarrow CH_4+H_2O$). However, CH_4 is not detected over the studied CeO_2 catalyst under test conditions. The other by-products are also not observed. These results indicate that only RWGS reaction occurs over the CeO_2 catalyst. The RWGS reaction is a reversible thermodynamic endothermic reaction. High temperature is conducive for RWGS reaction to obtain high CO_2 conversion and CO yield. The amount of active reactant molecules increases with the increase of the reaction temperature. This increase can improve CO_2 RWGS reaction at high temperature. Based on collision theory, high temperature can accelerate the rate of reactant molecule motion to enhance effective collision odds between active reactant molecules. This enhancement can advance the active CO_2 and H_2 molecules for RWGS reaction. Therefore, the CO_2 conversion increases with the increase of the reaction temperature over the CeO_2 catalyst in the RWGS reaction.

The catalyst preparation method has a significant effect on the structure of the obtained CeO_2 catalyst according to the XRD, TEM, and BET results. CO_2 RWGS reaction is a typical heterogeneous catalytic reaction. It involves the diffusion, adsorption, and surface reaction of the reactant molecules and the desorption of the product molecules. Thus, the structure of the prepared catalyst has a significant effect on catalytic performance of the CeO_2 catalyst in the CO_2 RWGS reaction. Based on the results of XRD, both the Ce-CA and Ce-PC catalysts have good crystallinity, which is not conducive to the activation of reactant molecules and the formation of surface oxygen vacancies. Based on the TEM and BET results, the Ce-CA and Ce-PC catalysts have low porosity and small specific surface area, which are not conducive to the absorption and activation of the reactant molecules. The Ce-HT catalyst has a developed porous structure according to the results of TEM and a large specific surface area of 144.9 $m^2 \cdot g^{-1}$, which is conducive to CO_2 and H_2 molecule adsorption and activation. Therefore, the Ce-HT catalyst shows excellent catalytic activity in the CO_2 RWGS reaction.

Surface oxygen species of CeO_2 can be reduced by H_2 to form oxygen vacancy, and the oxygen vacancy can be recovered in an oxidized atmosphere. Based on the results of the *in-situ* XPS and TPR, the surface oxygen species of CeO_2 can be reduced by H_2 to generate oxygen vacancy at the appropriate temperature. Moreover, CO_2 can react with oxygen vacancy according to the results of the *in-situ* XPS, which corresponds to the report of Wang et al. [11]. Therefore, a tentative mechanism is proposed for CO_2 RWGS reaction over the CeO_2 catalysts. This mechanism is as follows: (1) The surface oxygen species of CeO_2 in the H_2 atmosphere are reduced by H_2 to generate oxygen vacancies ($\square_{CeO2-\delta}$) (i.e., $H_2+CeO_2 \rightarrow H_2O+\square_{CeO2-\delta}$). (2) CO_2 molecules can oxidize oxygen vacancy and release CO (i.e., $CO_2+\square_{CeO2-\delta} \rightarrow CO+CeO_2$). Under the tested conditions, CeO_2 is reduced in high-purity H_2 stream at 400 °C for 2.0 h before RWGS reaction. The surface oxygen species of CeO_2 can be reduced by H_2 to generate oxygen vacancies. Subsequently, the reduced CeO_2 catalyst is exposed to feed gas ($H_2/CO_2/Ar=4:1:5$). CO_2 can oxidize oxygen vacancy to release CO. Reactant H_2 can reduce the surface oxygen species of CeO_2 to form $CeO_{2-\delta}$ and release H_2O. Thus, the RWGS reaction over CeO_2 catalyst is realized. Reactants, CO_2 and H_2, can be converted into CO and H_2O. The formed oxygen vacancies play a key role in the process of CO_2 RWGS reaction based on the tentative mechanism and the results of the *in-situ* XPS and TPR. Moreover, the formed oxygen vacancy is greater in the reduced CeO_2, which is more conducive to the conversion of CO_2 to CO. According to the TPR result, the Ce-CA catalyst reduced by H_2 at 400 °C generates very minimal oxygen vacancies, which is not conducive to the reduction of CO_2. The lowest RWGS reaction catalytic activity of the Ce-CA catalyst can be ascribed to very minimal oxygen vacancies. Some oxygen vacancies for the Ce-PC catalyst can be formed by H_2 reduction at 400 °C according to the results of TPR and *in-situ* XPS. The formation can improve CO_2 RWGS reaction. Thus, the Ce-PC catalyst has a relatively high RWGS reaction catalytic activity compared with the Ce-AC catalyst. Based on the results of TPR and *in-situ* XPS, the reducibility of the Ce-HT, Ce-CA, and Ce-PC catalysts at low temperature follows the order Ce-HT>Ce-CA>Ce-PC. The Ce-HT catalyst is reducible by H_2 at 400 °C to generate abundant oxygen vacancies. Thus, the Ce-HT catalyst shows an excellent catalytic performance in the CO_2 RWGS reaction. Based on the above results, the preparation method significantly affects the structure of the CeO_2 catalyst, thereby improving the catalytic performance in the CO_2 RWGS reaction. The formed oxygen vacancy also has a significant effect on the catalytic performance of the CeO_2 catalyst in the CO_2 RWGS. Thus, catalytic activity of the preparation CeO_2 catalyst in the CO_2 RWGS follows the order Ce-HT>Ce-PC>Ce-CA.

CONCLUSION

XRD, TEM, and BET characterizations indicated that the preparation method significantly affected the structure of the obtained CeO_2 catalysts. Based on the *in-situ* XPS and TPR results, the surface oxygen species of the prepared CeO_2 catalysts can be reduced by H_2 at 400 °C to generate oxygen vacancies. The formed oxygen vacancies can promote the reduction of CO_2 to obtain CO produc-

tion. The porous structure and a large specific surface area are conducive for H_2 molecules to adsorb and react with surface oxygen species on the surface of the CeO_2 to promote the formation of oxygen vacancies, thereby increasing the catalytic performance of the corresponding catalyst. The studied CeO_2 catalysts have 100% CO selectivity, and the catalytic activity in CO_2 RWGS reaction follows the order Ce-HT>Ce-PC>Ce-CA. The Ce-HT catalyst exhibited the highest CO_2 conversion and the CO_2 conversion can reach 15.9% at 580 °C. These results are promising to exploit efficient RWGS reaction catalytic system.

ACKNOWLEDGEMENTS

This research is funded by Science and Technology of Chongqing Municipal Education Commission funded research projects (No. KJ1500608); Student Innovation Fund of Chongqing Technology and Business University (No. 179029).

SUPPORTING INFORMATION

Additional information as noted in the text. This information is available via the Internet at http://www.springer.com/chemistry/journal/11814.

REFERENCES

1. G. Centi, E. A. Quadrelli and S. Perathoner, *Energy Environ. Sci.*, **6**, 1711 (2013).
2. G. L. Zhou, B. C. Dai, H. M. Xie, G. Z. Zhang, K. Xiong and X. X. Zheng, *J. CO_2 Utilization*, **21**, 292 (2017).
3. H. Ahmad, S. K. Kamarudin, L. J. Minggu and M. Kassim, *Renew. Sust. Energ. Rev.*, **43**, 599 (2015).
4. J. Yoshihara and C. T. Campbell, *J. Catal.*, **161**, 776 (1996).
5. T. Osaki, N. Narita, T. Horiuchi, H. Masuda, K. Suzuki and T. Sugiyama, *J. Mol. Catal. A: Chem.*, **125**, 63 (1997).
6. S. W. Park, O. S. Joo, K. D. Jung, H. Kim and S. H. Han, *Korean J. Chem. Eng.*, **17**, 719 (2000).
7. S. W. Park, O. S. Joo, K. D. Jung, H. Kim and S. H. Han, *Appl. Catal. A: Gen.*, **211**, 81 (2001).
8. D. H. Kim, S. W. Han, H. S. Yoon and Y. D. Kim, *J. Ind. Eng. Chem.*, **23**, 67 (2015).
9. H. Imagawa, A. Suda, K. Yamamura and S. H. Sun, *J. Phys. Chem. C*, **115**, 1740 (2011).
10. B. C. Dai, G. L. Zhou, S. B. Ge, H. M. Xie, Z. J. Jiao, G. Z. Zhang and K. Xiong, *Can. J. Chem. Eng.*, **95**, 634 (2017).
11. L. C. Wang, M. T. Khazaneh, D. Widmann and R. J. Behm, *J. Catal.*, **302**, 20 (2013).
12. Q. Q. Jiang, G. L. Zhou, Z. G. Jiang and C. Li, *Sol. Energy*, **99**, 55 (2014).
13. A. Goguet, S. O. Shekhtman, R. Burch, C. Hardacre, F. C. Meunier and G. S. Yablonsky, *J. Catal.*, **237**, 102 (2006).
14. B. W. Lu and K. Kawamoto, *Mater. Res. Bull.*, **53**, 70 (2014).
15. A. Goguet, S. O. Shekhtman, R. Burch, C. Hardacre, F. C. Meunier and G. S. Yablonsky, *J. Catal.*, **237**, 102 (2006).
16. A. Goguet, F. Meunier, J. P. Breen, R. Burch, M. I. Petch and A. Faur Ghenciu, *J. Catal.*, **226**, 382 (2004).
17. G. L. Zhou, H. Lan, H. Wang, H. M. Xie, G. Z. Zhang and X. X. Zheng, *J. Mol. Catal. A: Chem.*, **393**, 279 (2014).
18. G. L. Zhou, H. Lan, X. Q. Yang, Q. X. Du, H. M. Xie and M. Fu, *Ceram. Int.*, **39**, 3677 (2013).
19. G. L. Zhou, B. G. Gui, H. M. Xie, F. Yang, Y. Chen, S. M. Chen and X. X. Zheng, *J. Ind. Eng. Chem.*, **20**, 160 (2014).
20. P. Djinović, J. Batista and A. Pintar, *Catal. Today*, 147S, S191 (2009).
21. Z. P. Qu, F. L. Yu, X. D. Zhang, Y. Wang and J. S. Gao, *Chem. Eng. J.*, **229**, 522 (2013).
22. X. C. Fu and W. X. Shen, Physical Chemistry, Fifth Ed., High education press, Beijing (2006).
23. J. M. López, A. L. Gilbank, T. García, B. Solsona, S. Agouram and L. Torrente-Murciano, *Appl. Catal. B: Environ.*, **174-175**, 403 (2015).
24. Tana, M. L. Zhang, J. Li, H. J. Li, Y. Li and W. J. Shen, *Catal. Today*, **148**, 179 (2009).
25. A. Karpenko, R. Leppelt, J. Cai, V. Plzak, A. Chuvilin, U. Kaiser and R. J. Behma, *J. Catal.*, **250**, 139 (2007).
26. B. Choudhury, P. Chetri and A. Choudhury, *RSC Adv.*, **4**, 4663 (2014).
27. M. Nolan, S. C. Parker and G. W. Watson, *Surf. Sci.*, **595**, 223 (2005).
28. L. Z. Meng, S. L. Gong and Y. B. He, Chemistry Organic Spectral Analysis, 3rd Ed., Wuhan University Press, Wuhan (2009).
29. S. S Kim, K. H. Park and S. C. Hong, *Fuel Process. Technol.*, **108**, 47 (2013).
30. C. S. Chen, W. H. Cheng and S. S. Lin, *Chem. Commun.*, **18**, 1770 (2001).

Supporting Information

Reduction of CO_2 to CO via reverse water-gas shift reaction over CeO_2 catalyst

Bican Dai*, Shiquan Cao*, Hongmei Xie*, Guilin Zhou*,,†, and Shengming Chen***

*Chongqing Key Laboratory of Catalysis & Environmental New Materials, Department of Materials Science and Engineering, College of Environment and Resources, Chongqing Technology and Business University, Chongqing 400067, China
**Engineering Research Center for Waste Oil Recovery Technology and Equipment, Ministry of Education, Chongqing 400067, China
(*Received 19 June 2017 • accepted 25 September 2017*)

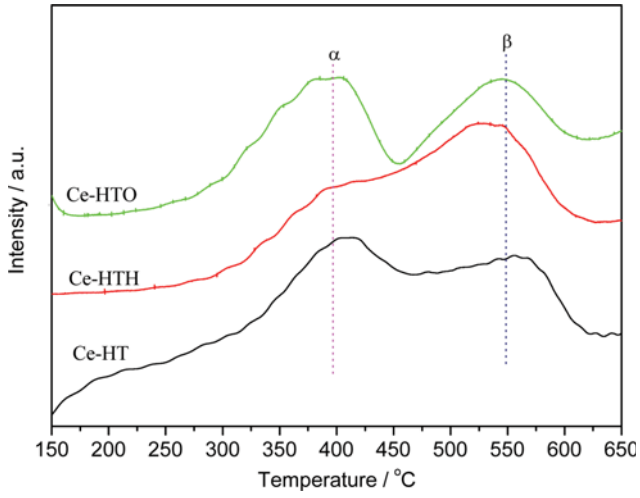

Fig. S1. H_2-TPR profiles of the Ce-HTO, Ce-HTH, and Ce-HT.